Organic & Biomolecular Chemistry

Accepted Manuscript

This article can be cited before page numbers have been issued, to do this please use: Ç. Çelik, N. Kakusho, T. Xu, S. S. Lee, N. Yoshizawa-Sugata, H. Masai and Y. Yamakoshi, *Org. Biomol. Chem.*, 2026, DOI: 10.1039/D6OB00581K.

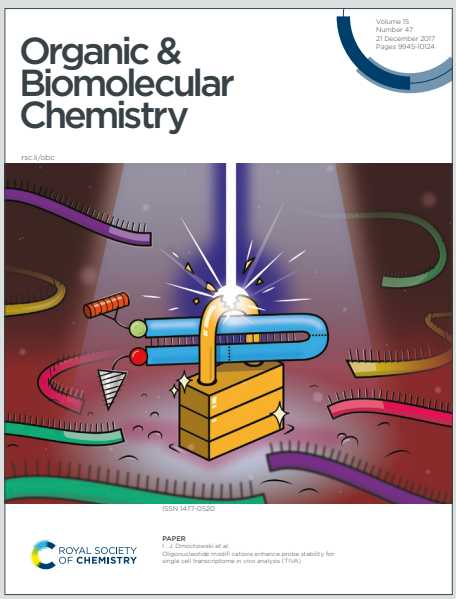

ROYAL SOCIETY OF CHEMISTRY

rsc.li/obc

View Article Online
DOI: 10.1039/D6OB00581K

ARTICLE

Linker dependence of $^1O_2$ generation by G4-binding tetra-imidazolium porphyrins

Received 00th January 20xx,
Accepted 00th January 20xx

DOI: 10.1039/x0xx00000x

Çetin Çelik,[a] Naoko Kakusho,[b] Tianyu Xu,[a] Sung Sik Lee,[c] Naoko Yoshizawa-Sugata, *[d] Hisao Masai*[b] and Yoko Yamakoshi *[a]

Three water-soluble porphyrins with tetra-cationic imidazolium groups were synthesized and assessed for complexation with human telomeric guanine-quadruplex (G4) DNA. By UV titration studies, these porphyrins showed 10-fold higher complexation stability to G4 DNA over non-G4 DNA. This was consistent with FRET experimental data showing G4 stabilization by these porphyrins was significantly enhanced in comparison to non-G4 DNA. The porphyrins had slightly longer wavelength of absorption in comparison to a previously reported cationic porphyrin with the same cationic groups but shorter linkers, indicating that they may be more suitable as photosensitizers (PSs) for photodynamic therapy (PDT). Significant photoinduced singlet oxygen ($^1O_2$) generation of these porphyrins was observed by ESR spin-trapping method under irradiation with deep red LED light (max at 660 nm). In the presence of telo24 G4 DNA, this photoinduced $^1O_2$ generation was enhanced. Cellular internalization of these porphyrins was observed by flow cytometry, resulting in sufficient photocytotoxicity of these porphyrins to both cancer cells (HeLa) and normal cells (NHDF). Photocytotoxicity to a cancer cell line was higher than to the normal cells. Although this mechanism was not clearly explained, the results show superior properties of these porphyrin molecules reported here as PDT-PSs.

Introduction

Cationic porphyrins, including TMPyP4, are often known as ligands for guanine-quadruplex (G4) DNAs.[1-4] G4s are one of the non-B secondary structures of DNA or RNA and observed in guanine (G)-rich sequences. In the presence of cations (*e.g.* K^+ and Na^+), four G bases form a tetrad structure *via* Hoogsteen-type hydrogen bonding and stacking with each other. Recently, G4s have been identified as potential therapeutic targets including cancers.[5, 6] For instance, promoter regions of many oncogenes, *e.g. MYC*, *VEGF*, *KRAS*, and *BCL2*, often contain G-rich sequences, which potentially form G4 structures. By stabilizing these G4s with specific ligands, the corresponding oncogenes can be downregulated.[7-9] Alternatively, G4 binders often inhibit telomerase, which plays an important role in the elongation of telomere repeats (TTAGGG).[10, 11] These telomere repeats are essential for the proliferation of cancer cells, resulting in the specific effects of G4-binders on cancer cells over normal cells. A number of G4 binders including porphyrin derivatives have been reported.

In addition to their G4-binding properties, porphyrins are known as efficient photosensitizers (PSs) for photodynamic therapy (PDT). PDT is a non-surgical treatment for various diseases including cancers, and majority of FDA-approved PDT-PSs are porphyrin derivatives. It involves PS molecules, visible light – ideally in the therapeutic window (650-800 nm) –[12] and molecular oxygen ($^3O_2$). Under visible light irradiation, porphyrins trigger the conversion of $^3O_2$ to singlet oxygen ($^1O_2$), a reactive oxygen species (ROS) to damage the tissues nearby.[13, 14] Recently, G4-targeting PSs have attracted attentions for selective treatment of cancer cells[15-22] due to their increased abundance of G4 DNA.[23-25] In addition, G is prone to the oxidation to form 8-oxo-guanine because of its lowest oxidation potential among all DNA/RNA bases.[26] Taken together, combining porphyrins tendency to localize in cancer,[27] the ability to use G4-binding porphyrins as a PS offers potential for selective treatment of cancer cells. Towards this aim, TMPyP4, a well-studied G4-binding porphyrin with photoinduced $^1O_2$ generation, was investigated for this application, but showed relatively low selectivity in binding to G4 over non-G4 DNA and low cellular uptake.[28]

Recently, we have reported two tetra cationic porphyrins, with tetra-guanidinium and tetra-imidazolium moieties.[26] These water-soluble porphyrins revealed both properties of G4 binding and photoinduced $^1O_2$ generation. In several *in vitro* tests, the porphyrin with tetra-imidazolium cations presented superior properties with higher binding stability to G4 DNA and

[a]*Department of Chemistry and Applied Biosciences, ETH Zürich, Vladimir-Prelog-Weg 3, CH-8093 Zürich, Switzerland. E-mail: yamakoshi@org.chem.ethz.ch*
[b]*Department of Basic Medical Sciences, Tokyo Metropolitan Institute of Medical Science, 2-1-6 Kamikitazawa, Setagaya, Tokyo 156-8506, Japan. E-mail: masai-hs@igakuken.or.jp.*
[c]*ScopeM, ETH Zürich, Otto-Stern-Weg 3, CH-8093 Zürich, Switzerland.*
[d]*Research Center for Genome & Medical Sciences, Tokyo Metropolitan Institute of Medical Science, 2-1-6 Kamikitazawa, Setagaya, Tokyo 156-8506, Japan. E-mail: yoshizawa-nk@igakuken.or.jp*
Supplementary Information available: [details of any supplementary information available should be included here]. See DOI: 10.1039/x0xx00000x

better cellular internalization in comparison to TMPyP4, resulting in enhanced photocytotoxicity to a cancer cell line over normal cells. In this study, we synthesized the tetra-imidazolium cationic porphyrins with longer linkers. We postulated that these tetra cationic porphyrins **1**-**3** (Fig. 1) may show improved properties in G4-binding and photosensitization due to their longer linkers. The synthesized porphyrins **1**-**3** were characterized in detail on their G4 stabilizing ability, photoinduced $^1O_2$ generation, photoinduced DNA damage, internalization to the cells, and photocytotoxicity, in comparison to the our previously reported porphyrin **4**.

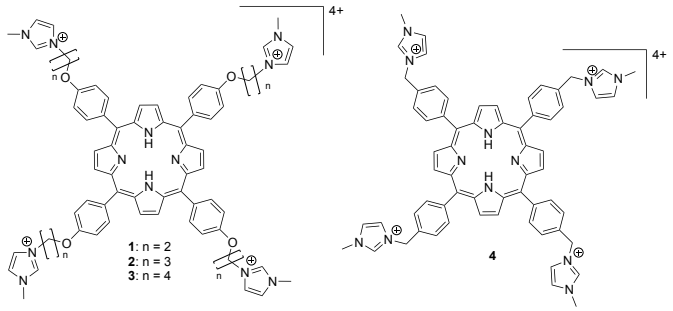

Fig. 1 Chemical structures of tetra cationic porphyrins **1**-**3** in this study and previously reported porphyrin **4**.

Results and Discussion

Syntheses of porphyrins 1, 2, and 3

Porphyrins **1**, **2**, and **3** were synthesized by standard method as shown in Scheme S1 in the ESI. The porphyrins **S4** – **6**, were prepared from aldehydes **S1** – **3** and pyrrole *via* the Lindsey method, and converted to porphyrins **1** – **3** by a nucleophilic addition of 1-methyl imidazole. The resulting porphyrins were purified by a reverse phase HPLC and treated with Dowex for anion exchange to provide Cl^- salts revealing a single peak by HPLC (Figs. S17, S25, and S33). Porphyrins **1**, **2**, and **3** were characterized by ^1H, ^{13}C NMR, HRMS, FT-IR-ATR to clearly confirm their structures (data are in the ESI). By HRMS measurements, molecular ion peaks corresponding to *m/z* of M^{4+}, $[M–H]^{3+}$, and $[M+H]^{5+}$ were observed for all three porphyrins (Figs. S15, S23, and S31). UV-vis spectra revealed one Soret band and four Q-bands in line with typical characteristics for metal-free porphyrins (Fig. 2a). Both the Soret band and the Q-bands of porphyrins **1** – **3** were red-shifted in comparison to our previous imidazole porphyrin **4**,[29] presumably due to the O-atoms connected to aromatic rings. Especially, the longest Q-band observed for each porphyrin **1** – **3** was at a maximum ca 654 nm, significantly shifted to a longer wavelength in comparison to **4**, which has a maximum at ca 640 nm (Fig. S42). This red shift in excitation wavelength of PS is advantageous for PDT, which requires light source with longer wavelengths due to their better tissue penetration. A slight increase in absorption intensity of the longest Q-band was observed upon increase of linker length (**1** < **2** < **3**). All porphyrins were fluorescent as shown in Fig. 2b.

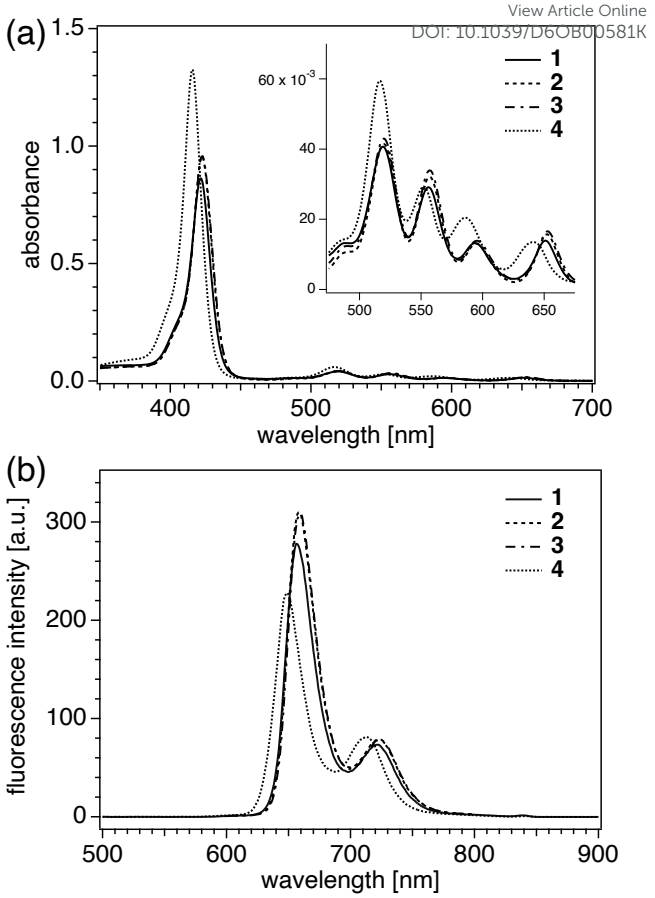

Fig. 2 (a) UV-vis of porphyrins **1** – **4**. (b) Fluorescence spectra of porphyrins **1** – **4** using excitation wavelength of 423 nm and 5 nm of slit. All measurements were conducted with 5 μM solutions in pH 7.4 HEPES buffer (10 mM).

Fluorescence titration

The interactions of porphyrins **1** – **3** with G4 DNA were initially investigated by fluorescence spectra (Fig. 3). The telo24 G4 DNA with a hybrid (3+1) structure was used. To a solution of each porphyrin (5 μM) in pH 7.4 HEPES buffer (containing 100 mM KCl to induce a hybrid (3+1) conformation), G4 was added at varied concentrations. As shown in Fig. 3a, upon addition of G4 DNA, the fluorescence intensity of each porphyrin **1** – **3** decreased in a dose-dependent manner, indicative of interaction between porphyrin and G4. By Stern-Volmer plots, the highest K_q was observed in the case of porphyrin **1** with the shortest linkers (Fig. 3c). Interestingly, the fluorescence quenching was much more significant in comparison to the previously reported porphyrin **4**.[29]

DOI: 10.1039/D5OB00581K

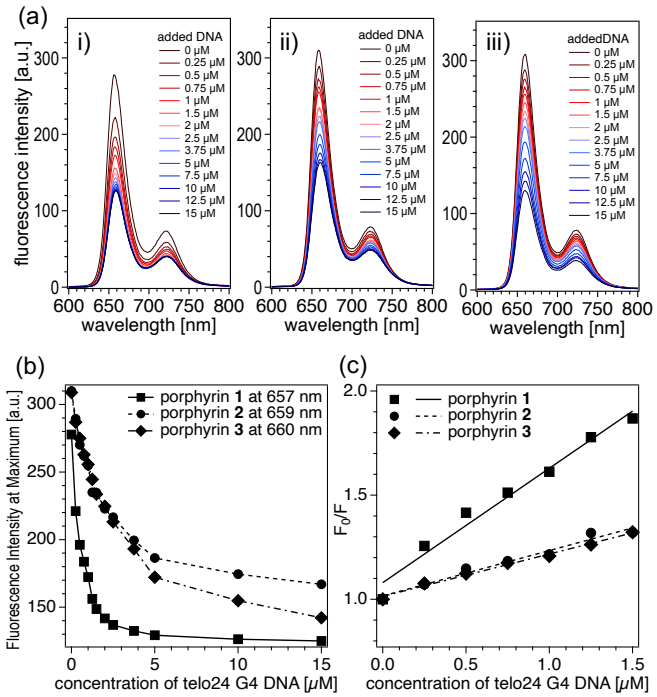

Fig. 3 Fluorescence spectra of porphyrins **1** – **3** upon addition of telo G4 DNA. (a) Fluorescence spectra of porphyrins **1** – **3** (5 μM) in the presence of varied concentrations of telo24 G4 DNA (0-15 μM). (b) Dose-dependent decrease of fluorescence intensity of porphyrins **1** – **3** at emission maxima. (c) Stern-Volmer plot of fluorescence quenching of porphyrins **1** – **3**. Measurements: in pH 7.4 HEPES (10 mM) containing 1 mM Na_2EDTA and 100 mM KCl; excitation wavelength: 423 nm; slit width: 5 nm.

UV-vis titration

To assess the binding stability of porphyrins **1** – **3** and G4, UV-vis spectra of porphyrins in the presence of varied concentration of G4 were measured. As seen in Fig. 4, similar spectral changes were observed in all porphyrins **1** – **3** upon addition of telo24 G4 DNA with significant intensity decrease of Soret band. While porphyrins **1** and **2** with shorter linkers showed slight red shift in Soret band, porphyrin **3** with longer linkers revealed no significant shift. These changes were similar to our previously reported porphyrin **4** and other porphyrins with shorter linkers.[29, 30]

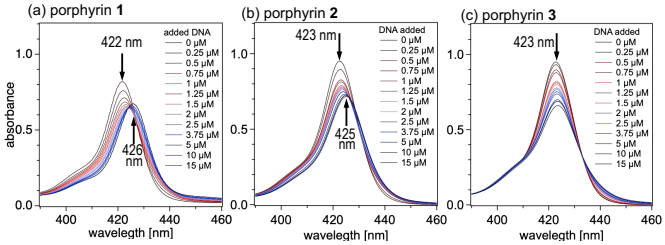

Fig. 4 Interaction of porphyrins **1** – **3** with telo G4 DNA by UV-vis absorption spectra. (a) near the Soret band of **1**, **2** and **3** (5 μM) in 10 mM HEPES (pH 7.4 with 1 mM Na_2EDTA and 100 mM KCl) in the presence of telo24 G4 DNA (0-15 μM).

From the UV data, K_d values for complexation of porphyrins to telo24 G4 were determined (Figs. S35 and S38, Table 1). As a control, hairpin DNA (hpDNA) with non-G4 structure was employed. As shown in Table 1, significantly lower K_d values were obtained in the case of G4 DNA compared to the control hpDNA in all porphyrins. Among porphyrins **1** – **3**, porphyrin **1** with shortest linkers showed the highest complexation stability with G4 DNA (K_d = 0.72 μM). However, complexation stability with G4 was lower than our previous porphyrin **4** although in a similar range. Elongation of the linkers did not contribute to the enhancement of complexation stability.

Table 1 K_d values of binding of porphyrins **1** – **4** with telo24 G4 DNA and hairpin (non-G4) DNA obtained from UV-vis titration data

compounds	K_d (SE) [μM][a]	
	telo24 G4 DNA	hairpin DNA
1	0.72 (0.07)	6.39 (0.56)
2	1.09 (0.18)	11.47 (1.30)
3	2.28 (0.31)	10.75 (1.26)
4	0.34 (0.07)	6.67 (0.87)

[a] Obtained using linear regression on the binding model developed by Wolfe et al.[31] using GraphPad Prism 8 software (Figs. S35 and S38 in the ESI).

FRET melting assay for G4-stabilization effects

The fluorescence and UV-vis measurement assays above indicated potential interactions between the porphyrins **1** – **3** and G4 DNA (Figs. 3 and 4). To further evaluate these interactions, the stabilization effects of the porphyrins on telo24 and Rif1-2 G4 DNAs were studied. Rif1-2 G4 DNA is a recently identified G4-forming sequence and known to bind to replication timing regulatory factor 1 protein (Rif1).[32, 33] FRET melting assays were conducted by monitoring FAM emission from dual-labelled telo24 or Rif1-2 G4 DNA in the presence of each of porphyrin **1** – **3**. In FRET assay, with temperature increase, G4 structure is disrupted, resulting in a decreased FRET efficiency and a concomitant increase in FAM emission. And as results, the addition of the porphyrins led to a dose-dependent decrease in FAM emission and a corresponding increase in the melting temperature (Tables S39 and S40).

As shown in Fig. 5a, porphyrin **1** showed a stabilization effect on telo24 G4 at above 0.3 μM, to an extent that shown by TMPyP4, a standard G4 binder. In contrast, porphyrin **3** required higher doses to achieve stabilization, while **2** exhibited the least stabilizing effect. Rif1-2 G4 DNA, a less stable G4 than telo24, was significantly stabilized by porphyrin **1** at 0.3 μM (ΔT_m: 46°C) and maximally stabilized at ≥ 0.6 μM (ΔT_m: >65°C), effect similar to that by TMPyP4. Higher concentrations of **2** and **3** were required to stabilize Rif1-2 G4 DNA, mirroring the trend observed with telo24.

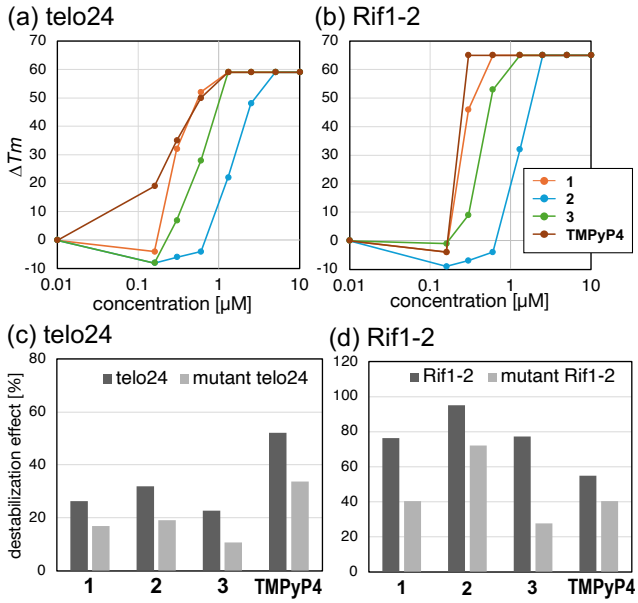

Fig. 5. The stabilization of G4 DNA by **1** – **3** and G4 specificity analysed by FRET assay. (a, b) The change of Tm values (ΔT_m) of telo24 (a) or Rif1-2 (b) G4 DNA in the presence of **1**, **2**, **3**, or TMPyP4 was plotted (the experiment without the compounds was used as a standard). (c, d) The normalized FAM emission signals of the labelled telo24 (c) or Rif1-2 (d) G4 (0.2 μM) in the presence of compound **1**, **2**, **3**, or TMPyP4 and competitor (5 μM) wild-type G4 DNA (dark grey) or mutant G4 DNA (light grey).

Given that some of the known G4 binders are non-specific and interact also with non-G4 DNA, developing selective binders is crucial, especially to target the physiological G4s on the highly transcribed genomes or in rapidly cycling cancer cells. To this end, we performed FRET assays in the presence of two competitors, G4 or non-G4 DNAs, to assess the G4 selectivity of our compounds. All compounds **1** – **3** demonstrated G4-selectivity for the telo24 DNA during the thermal shift (Figs. S39 and S40, a to d). The G4 selectivity rates for **1**, **2**, and **3** were 1.6, 1.7, and 2.1, respectively, comparable to or slightly better than that of TMPyP4 (1.5) (Fig. 5c; Figs, S41, a to d; Table S3). Interestingly, the G4 selectivity rates for the Rif1-2 for **1** and **3** were significantly higher (1.9 and 2.8, respectively) compared to TMPyP4 (1.4) (Fig. 5d, Fig. S41, and Table S4). These results suggested that our porphyrin compounds may exhibit preferences for specific G4 DNA topologies. CD spectra indicate Rif1-2 is likely to be parallel-type, whereas telo24 is hybrid and/or anti-parallel type.[33, 34] Porphyrins **1** – **3** may have preference for parallel-type, which is often the case for G4 binding proteins *in* vivo. Notably, a prominent feature in the FRET melting curves was observed around 75 °C, particularly in the presence of compound **3** (Fig. S41c and g). While this indicates a potential compound-induced structural transition at elevated temperatures, the G4-selectivity analysis was primarily conducted at $Temp_{\Delta max}$ (see Fig. S42) mostly below 60 °C to ensure quantitative comparisons during the main melting transition. The detailed mechanism behind the high-temperature behavior of compound **3** remains a subject for future investigation.

Photoinduced $^1O_2$ generation by porphyrins 1 – 3

Photoinduced generation of $^1O_2$ by the porphyrins were investigated by ESR using 4-oxo-TEMP as a spin-trapping agent. In the presence of $^1O_2$, 4-oxo-TEMP forms adduct, 4-oxo-TEMPO, that shows specific signals in the ESR.[35] The obtained ESR signals were quantified to evaluate the amount of $^1O_2$ generated. To be consistent with suitable condition for PDT, deep-red LED light (maximum at 660 nm) was used. Upon photoirradiation, porphyrins **1** – **3** generated $^1O_2$ significantly with a slightly higher amount in the case of porphyrin **2** (Fig. 6a-c). The $^1O_2$ generation by **1** – **3** were about double to that observed with previously reported porphyrin **4**. By taking into account the absorption intensity of **1** – **3** at 660 nm was about 2.0 – 2.7 times higher than **4**, photosensitivity of all porphyrins **1** – **4** were in a similar range (Fig. S42).

Notably, in the presence of telo24 G4 DNA, photoinduced $^1O_2$ generation by porphyrins **1** – **3** were highly enhanced (Fig. 6a-d, iii). In the presence of 1 equiv of telo24 G4 DNA to each porphyrin, $^1O_2$ generation was increased by 1.3 – 1.5 times in comparison with the conditions using only the porphyrin. These enhanced $^1O_2$ generation was not significantly observed in the presence of a non-G4 DNA (hpDNA). By UV-vis measurements, no significant intensity increases at 660 nm in the mixtures of porphyrins **1** – **3** and telo24 were observed. The enhanced $^1O_2$ generation observed here may be related to the microenvironment of porphyrins interacting with G4 DNA to be favor in $^1O_2$ generation in the steps in *type II* energy transfer reaction *e.g.* in photoexcitation or intersystem crossing. Nevertheless, generation of $^1O_2$ by porphyrins **1** – **3** was significantly higher than previously reported **4** and TMPyP4 under 660 nm light with further enhancement in the presence of G4 DNA, indicating their superior properties as PDT-PSs.

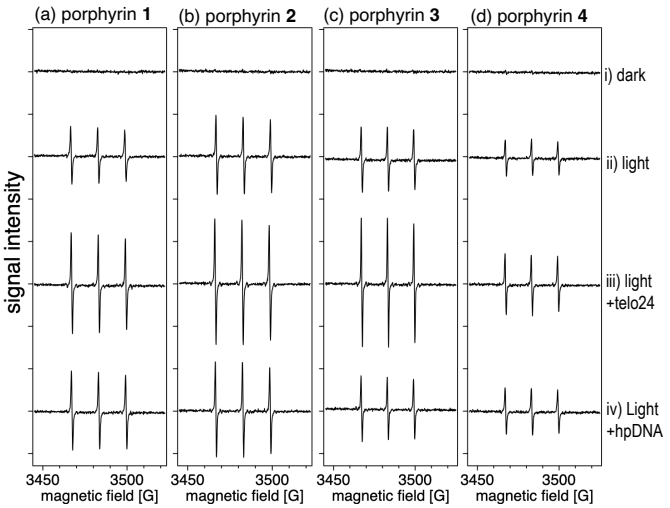

Fig. 6 X band ESR spectra of $^1O_2$ adduct of 4-oxo-TEMP in the porphyrin solutions observed under irradiation of visible light (maximum at 660 nm) for 10 sec. Conditions: porphyrin: 50 μM; 4 oxo TEMP: 80 mM, KCl: 100 mM, DNA: 50 μM in 10 mM HEPES buffer pH 7.4.

View Article Online DOI: 10.1039/D5OB00584K

Table 2 Effect of G4- and non-G4 DNAs on photoinduced $^1O_2$ generation by porphyrins **1 – 4**

PSs	amounts of generated 4-oxo-TEMPO relative to compound **4**[a]		
	PS only control	telo24 G4 DNA (relative to control)	hairpin DNA (relative to control)
1	1.98	2.95 (1.49)	2.14 (1.08)
2	2.16	3.54 (1.64)	2.39 (1.11)
3	1.82	2.44 (1.34)	1.83 (1.01)
4	1.00	1.65 (1.65)	1.16 (1.16)

[a] Relative amount of 4-oxo-TEMPO, $^1O_2$ adduct of 4-oxo-TEMP, observed by ESR calculated from the double integration of ESR signal (Fig. 6).

Photoinduced DNA cleavage

Photoinduced DNA damage by porphyrins **1 – 4** was tested on pBR322 supercoiled DNA under visible light irradiation (660 nm LED). The pBR322 DNA, which has numerous potential G4 ligand binding sites (20 potential G4 sites predicted by QGRS (quadruplex forming G-rich sequences) Mapper[36]), was used as a substrate DNA, as it is often employed in the assays for oxidative damages of DNA by the photosensitizers. The formation of nicked DNA (form II) was quantified by electrophoresis stained with GelRed®nucleic acid stain and analyzed by ImageJ. Porphyrins **1 – 3** showed a similar level of photoinduced DNA cleaving activity with IC_{50} of 0.11, 0.11, 0.13 μM, while control porphyrin **4** showed much reduced effect with IC_{50} 0.57 μM (Fig. 7). The result showed a similar trend to that amount of $^1O_2$ generation (Fig. 6).

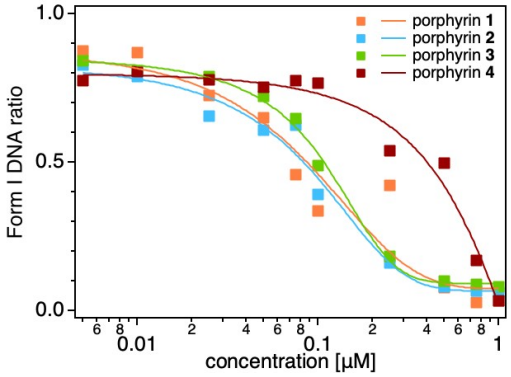

Fig. 7 Concentration-dependent photoinduced DNA cleavage by porphyrins **1**, **2**, **3**, and **4**. The pBR322 supercoiled DNA was used and ratio of form I intact DNA were quantified by ImageJ. Irradiation conditions: light: deep-red LED (maximum at 660 nm); pBR322 DNA: 12.5 μg•mL^{-1}; in Tris–HCl-EDTA buffer (pH 8.0); for 10 min.

Internalization of porphyrins into the cells

Cellular uptake of PS molecules is an important factor for their function as both G4 binders and PDT-PSs. Taking advantages of the fluorescence intensity of porphyrins **1 – 3**, cellular uptake of the molecules was assessed by flow cytometry using both a cancer cell line (HeLa) and normal cells (NHDF). The cells were co-incubated with each of porphyrin **1 – 3** (10 μM) for 24 h. Subsequently, the cells were washed with PBS(–) and treated with trypsin to prepare cell suspension, which was washed again before subjected to flow cytometry. A laser excitation of 405 nm and a detection filter of 678 - 706 nm were used, since all porphyrins **1 – 3** have almost identical excitation and emission co-efficient at these wavelength regions.

Fig. 8 shows flow cytometry histograms for the internalization of each porphyrin. Among three porphyrins, the cells treated with porphyrin **3** had the highest fluorescence intensity, which was followed by **2** and **1**, indicating that cell internalization efficiency of the porphyrins was **3** > **2** > **1** in both cells. This may be related to the lipophilicity of the porphyrin molecules –porphyrin **3** containing longest alky linkers with highest lipophilicity shows higher cellular uptake due to better interaction with lipid membrane of the cells. The mean fluorescence intensities of porphyrins **1 – 3** obtained by flow cytometry were higher than our previously reported porphyrin **4**, that has shorter linkers with internalization efficiency of 1.0 x 10^5 and 3.5 x 10^5, respectively, for HeLa and NHDF (summarized in Table S1). Results showed clearly that elongation of the linkers significantly improved cellular internalization, making the compounds advantageous as G4-targeting drugs and PDT-PS.

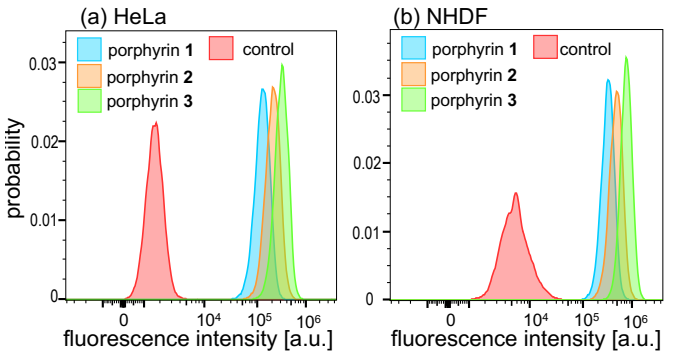

Fig. 8 Flow cytometry histogram for cellular internalization of porphyrins **1, 2** and **3** in HeLa (a) and NHDF (b). The normalized histograms show the fluorescence observed cells incubated at 10 μM concentration of porphyrin (Ex: 405 nm, Em: 678 - 706 nm).

Photocytotoxicity

Encouraged by results of cellular uptakes of porphyrins **1 – 3** above, photocytotoxicity tests were conducted on both HeLa and NHDF cells. After the co-incubation with each porphyrin for 2 h at varied concentrations, cells were washed and irradiated by deep red LED light (max 660 nm) for 15 min and subjected to MTT assay for cell viabilities. As a control, previously reported porphyrin **4** was tested under the same conditions. Fig. 9 shows a clear dose-dependent effect of each porphyrin on cell viabilities. IC_{50} values were calculated and summarized in Table 3. As seen in Fig. 9, all of porphyrins **1 – 4** showed significant cytotoxicity under visible light irradiation. Slight dark toxicity was observed in porphyrins especially with longer linkers. All compounds showed higher photocytotoxicity to HeLa cells than to NHDF cells. Photocytotoxicity of porphyrins **1 – 3** were much efficient with lower IC_{50} values than our previously reported porphyrin **4**, in line with above-mentioned (1) more efficient generation of $^1O_2$ under deep-red light irradiation (max 660 nm) and (2) better cell internalization effect. Higher phototoxicity to HeLa in comparison to NHDF may be related to higher abundance of G4 DNA domains in HeLa compared to normal

cells, although this relationship is still unclear. Nevertheless, the results suggest that these porphyrins may be potentially effective in selective damage of cancer cells under visible light irradiation.

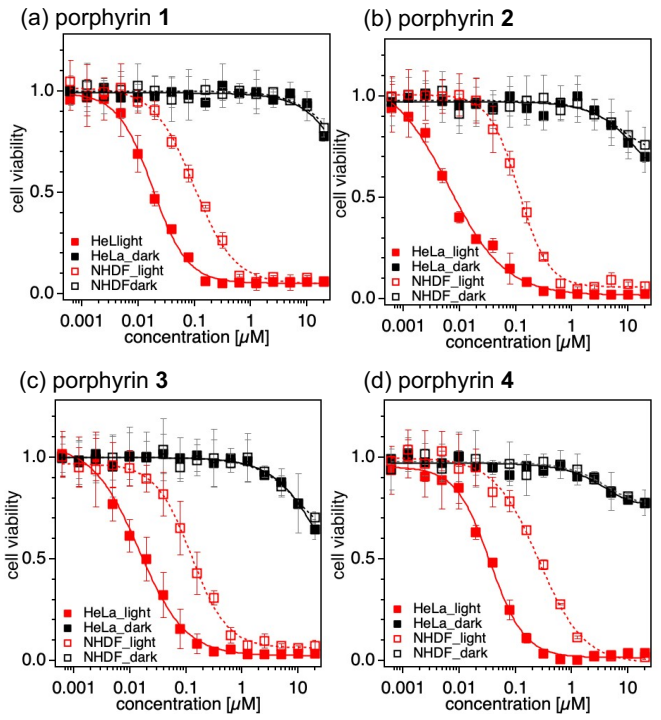

Fig. 9 Photocytotoxicities of porphyrins **1** (a), **2** (b), **3** (c) and **4** (d) under irradiation of deep red LED (λ_{max} = 660 nm, for 15 min) on HeLa and NHDF cells measured by MTT assay.

Table 3 IC_{50} values for photoinduced cytotoxicity of porphyrins **1** – **4**

compounds	IC_{50} (SE) [nM][a]	
	HeLa	NHDF
1	17.9 (1.1)	97.5 (7.3)
2	6.4 (1.3)	113.6 (4.8)
3	14.5 (1.5)	124.5 (7.1)
4	35.4 (3.1)	260.7 (24.8)

[a] Values were obtained from Hill equation fitting of the data points shown in Fig. 9 by Igor Pro 10 software.

Confocal Microscopy of Permeabilized Cells

To identify the interaction of porphyrins **1 – 3** with cellular components, confocal microscopy measurements were conducted on HeLa and NHDF cells. Cells were permeabilized by detergent and fixed prior to the coincubation with porphyrins. Permeabilized cells were treated with each porphyrin (5 μM), washed, and imaged on a confocal microscope with an excitation wavelength of 405 nm and emission filter of 660 – 735 nm to observe the localization of the porphyrins by fluorescence (Fig. 10). All porphyrins **1** – **3** showed similar localization patterns. In HeLa cells, localization of all three porphyrins was observed as stronger signals in the nucleoli as well as in the cytosolic regions. In NHDF cells, fluorescence signals were spread throughout the cell with punctuated signals in the cytosol shown by emissions, while there was no significant emission in nuclei. The signal observed from the nuclei of the HeLa cells may be related to the interaction of the porphyrins **1 – 3** with G4 DNA, which are more abundant in cancer cells.

View Article Online
DOI: 10.1039/D6OB00591K

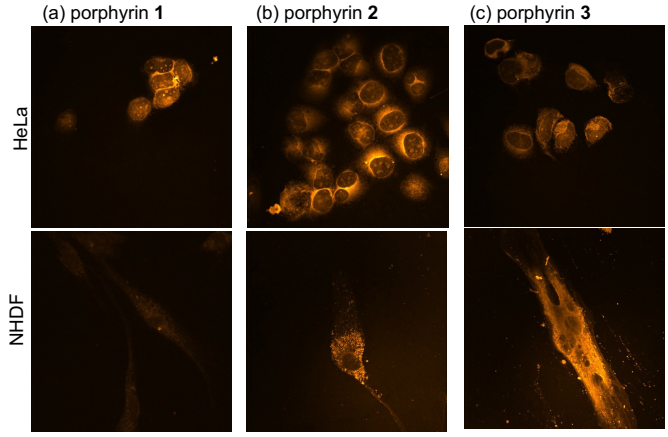

Fig. 10 Confocal microscopy images of HeLa cells and NHDF cells pre-treated with 0.5% Triton X-100 for permeabilization and subsequently co-incubated with 5 μM solution of porphyrins **1**, **2** or **3** (excitation: 405 nm, filter: ET700/75, image size: 140 x 140 μm).

Experimental

Fluorescence spectroscopy. Fluorescence spectroscopies were recorded on a Varian Cary Eclipse spectrophotometer (Agilent Technologies, Inc., Santa Clara, California, U.S.). Each solution of **1**, **2**, or **3** (5 μM) was prepared in 10 mM HEPES buffer (pH 7.4, containing 100 mM KCl and 1 mM Na_2EDTA). A solution of single strand telo24 DNA (500 μM) with the sequence of d(TTAGGGTTAGGGTTAGGGTTAGGG) was prepared in same buffer and subjected to the pre-annealing process by heating at 90 °C for 10 min and cooling back to room temperature over 3 h. To each porphyrin solution (2 mL) in a quartz cuvette (path length: 1 cm), an aliquot of the DNA solution was added and left to equilibrate for 2 min upon mixing to record fluorescence spectra.

UV-Vis. UV Absorption spectra were recorded on a JASCO V-570 UV/VIS/NIR spectrophotometer (JASCO Co., Tokyo Japan). Each solution of **1**, **2** or **3** (5 μM) was prepared in 10 mM HEPES buffer (pH 7.4, containing 100 mM KCl and 1 mM Na_2EDTA). A solution of single strand telo24 DNA (500 μM) with the sequence of d(TTAGGGTTAGGGTTAGGGTTAGGG) was prepared in same buffer and subjected to the pre-annealing process by heating at 90 °C for 10 min and cooling back to room temperature over 3 hours. To each porphyrin solution (2 mL) in a quartz UV cuvette (path length: 1 cm), an aliquot of the DNA solution was added and left to equilibrate for 2 min upon mixing to record UV-vis spectra. The titration was stopped when there was no change observed upon addition of DNA.

FRET melting assay. G4 stabilization by porphyrins was assessed by FRET assay using telo24 and Rif1-2 DNA labeled with 6-carboxyfluorescein (FAM) at 5’ - end and tetramethyl-rhodamine (TAMRA) at 3’ -end (Fasmac Co., Ltd., Kanagawa, Japan). The details are described in the SI.

DOI: 10.1039/D5OB02015K

Detection of $^1O_2$ by ESR spin trapping reagents. ESR spectra were recorded on a Bruker EMX, Continuous Wave X-Band EPR spectrometer (Bruker BioSpin GmbH). Each measurement was performed on the sampls in a Blaubrand® intraMark capillary (50 µL, Brand GMBH, Wertheim, Germany) placed inside a Suprasil® ESR tube (diameter: 4 mm, length: 250 mm, wall thickness: 0.8 mm; SP Wilmad-Lab Glass, NJ, USA). The 2,2,6,6-tetramethylpiperidin-4-one (4-oxo TEMP) was purchased from ABCR (Karlsruhe, Germany) and purified prior to use by sublimation. Nunc MicroWell 96 Well Round (U) Bottom Plate was bought from Thermo Scientific (Waltham, MA, USA). Lumidox® II 96-well LED Array (Analytical Sales and Services, Inc., NJ, USA) equipped 660 nm max LED was used for light irradiation. DNA oligonucleotides were purchased from Integrated DNA Technologies, Inc. (Coralville, IA, USA). Telo24 G4 DNA with the sequence of d(TTAGGGTTAGGGTTAGGGTTAGGG) was subjected to the pre-annealing process by heating at 90 °C for 10 min and cooling back to room temperature over 3 hours in 10 mM HEPES buffer (pH 7.4, containing 100 mM KCl and 1 mM Na_2EDTA). All measurements were conducted in the same buffer conditions.

DNA photocleavage assay. The pBR322 DNA and Gel Loading Dye, Purple (6X) were purchased from New England Biolabs (Ipswich, MA, USA). Nunc MicroWell 96 Well Round (U) Bottom Plate was bought from Thermo Scientific (Waltham, MA, USA). Ethylenediaminetetraacetic acid disodium salt dihydrate (EDTA), GelRed® Nucleic Acid Stain 10000X and agarose were purchased from Sigma-Aldrich (St. Louis, MI, USA). Lumidox® II 96-well LED Array (Analytical Sales and Services, Inc., NJ, USA) equipped with 660 nm max LED was used for light irradiation. Gel Electrophoreses were performed using Mupid-exU gel electrophoresis system (Mupid Co. Ltd., Tokyo, JAPAN). Imaging of the gels were performed using ChemiDoc Imaging System (Bio-Rad Laboratories, Inc., CA, USA).

The pBR322 DNA was diluted to a stock solution of 25 ng•µL–1 in Tris-HCl buffer (10 mM, pH 8.0, containing 1 mM EDTA). An aliquot of DNA solution (10 µL) was mixed with 10 µL solution of **1**, **2**, **3** or **4** in Milli-Q water. The mixtures were irradiated by 96-well illuminator for 10 min by the light source of 660 nm deep red LED (330 mW•cm^{-2}). Subsequently, Gel Loading Dye Purple 6X (4 µL) was added to each sample to be loaded to an agarose (1% agarose in 0.5X TBE buffer). Electrophoreses were conducted at 100 V for 80 min using 0.5X TBE as the running buffer. The gel was then stained using GelRed® Nucleic Acid Stain 3X (diluted from 10000X by milliQ water) for 1 h. The gels were then imaged using GelRed filter settings to provide the images. The images were analyzed using ImageJ software

Cell culture. HeLa and NHDF cells were purchased from ATCC (Manassas, VA, USA). The cells were incubated in DMEM containing 10% FBS supplemented with 2 mM glutamine and 1% penicillin-streptomycin. The pre-cultured semi-confluent cells were dispersed by trypsin and used for the experiments. The following materials were obtained from Thermo Fisher Scientific Inc. (Waltham, Massachusetts, USA): Gibco™ DMEM High Glucose; Gibco™ DMEM high glucose, no glutamine, no phenol red; Gibco™ Fetal Bovine Serum (FBS); Gibco™ Trypsin-EDTA 0.05%, PBS(–) (pH = 7.4, Mg^{2+}, Ca^{2+} free); 200 mM glutamine; Triton X-100; Gibco™ penicillin-streptomycin (10000 U•mL^{-1}).

Flow cytometry. HeLa and NHDF cells were inoculated in a 6-well plate with a density of 3x10^6 cells per well and incubated in DMEM containing 10% FBS and 1% penicillin-streptomycin for 24 h. Subsequently, the cells were incubated in the presence of 10 µM of each porphyrin for additional 24 h. Cells were trypsinized and centrifuged and obtained pellets were washed with PBS(–) for three times and resuspended in PBS(–) (500 µL) for measurement. Flow cytometry measurements were performed on Cytek® Aurora system (Cytek Biosciences, Fermont, CA, USA). Data were analyzed using FlowJo software with the V12 channel (excitation wavelength: 405 nm; emission wavelength: 692 nm (center) with 28 nm width).

Photocytotoxicity Assay. The 3-(4,5-dimethylthiazol-2-yl)-2,5-diphenyltetrazolium bromide (MTT) and Tween-20 were purchased from Sigma-Aldrich Co. (St. Louis, MI, USA). All cells were incubated in Gibco™ DMEM High Glucose containing 10% FBS and 1% penicillin-streptomycin. The 96-well plates were purchased from (Techno Plastic Products AG, Trasadingen, Switzerland). Lumidox® II 96-well LED Array (Analytical Sales and Services, Inc., New Jersey, USA) equipped with deep red LED (660 nm max) was used for photoirradiation. The cell viabilities were evaluated by MTT assay in which OD_{560} was measured using a microplate reader (infinite F200PRO, Group Ltd., Zürich, Switzerland). The means of at least three independent experiments were reported and all cell viability results are expressed as means ± SE.

Photocytotoxicity of **1**, **2**, **3**, and **4** and were tested on HeLa and NHDF cells. Preincubated cells were harvested and seeded to a 96-well plate with a density of 1000 cells per well (100 µL) and cultured for 24 h in an incubator at 37 ºC in presence of 5% CO_2 atmosphere. The growth medium in each well was then exchanged with medium containing each compound and the cells were incubated under the same conditions for 2 h. Afterwards, cells were washed with PBS(–) and phenol red-free DMEM was added to each well. The cells in 96-well plates were then illuminated for 15 min using 660 nm max deep red light (330 mW/cm2). After the illumination, DMEM media were exchanged with MTT solution in phenol red-free DMEM (0.5 mg•mL^{-1}, 100 µL) and cells were further incubated for 3 h. Subsequently, the media was removed from each well to be replaced with DMSO (100 µL). OD_{560} values were measured by the plate reader. Cell viabilities were calculated from OD560 values relative to negative control where the cells were not treated with any chemicals and positive control where the cells were treated with Tween-20.

Confocal microscopy. All cells were incubated in Gibco™ DMEM High Glucose containing 10% FBS and 1% penicillin-streptomycin. Semi-confluent cells were trypsinized and seeded onto ibidi™ µ-Slide 8 Wells at 10000 cells in 250 µL density. Cells were incubated in growth medium for 24 h. Subsequently, cells were permeabilized using 0.5% Triton X-100 and fixed using 4% PFA. Afterwards, HeLa and NHDF cells were incubated in the presence of porphyrin solution in PBS(-) for 5 min, washed with

PBS(-) and observed under microscope. Excitation: 405 nm laser, emission filter: ET700/75.

Conclusions

In summary, three porphyrin molecules **1** – **3** possessing four imidazolium moieties connected with different lengths of linkers were synthesized as potential G4-targeting PSs. The synthesized porphyrins **1** – **3** showed G4 binding ability with better selectivity in comparison to the control porphyrin **4**, as indicated by fluorescence, UV-vis titration, and FRET assay. Among these porphyrins, compound **1** with the shortest linker length displayed the strongest binding to telo24 DNA but effect was weaker than control porphyrin **4**. Upon elongation of linkers, however, selectivity of interaction to G4 DNA over non-G4 DNA was significantly increased in both telo24 and Rif1-2 G4s. All porphyrins **1** – **3** revealed $^1O_2$ generation under deep-red light irradiation (660 nm) evident from ESR spin trapping method at a higher level than control porphyrin **4**. Interestingly, in the presence of telo24 G4 DNA, enhanced $^1O_2$ generation was observed in comparison to the case in its absence. Efficient cellular uptakes of the porphyrins were indicated by flowcytometry, and photocytotoxicities are correlated with the efficiency of cellular uptake. As results, porphyrins **1** – **3** reported here revealed superior properties in comparison with previously reported porphyrin **4** and standard G4 binder TMPyP4 and can be considered as a potential core structure for further development of G4 targeted PDT-PSs.

Author contributions

N.Y.-S., H.M., and Y.Y. designed the overall project. C.C. designed detailed structures of the molecules and contributed to their synthesis and structural characterization in collaboration with Y.Y. N.K. and N.Y.-S. performed FRET assay in collaboration with H.M. C.C. performed fluorescence, UV-vis, and CD spectroscopy, ROS generation assay by ESR, DNA cleavage tests, and photocytotoxicity assay in collaboration with Y.Y. C.C. preformed fluorescence microscopy analyses in collaboration with S.-S.L. T.X. performed flow cytometry assay in collaboration with C.C. The manuscript was written with contributions of all authors. All authors have given approval to the final version of the manuscript.

Conflicts of interest

There are no conflicts to declare.

Data availability

Supplementary information: experimental data and details regarding the synthesis, ESR, UV-vis, fluorescence and flow cytometry, DNA photocleavage, photocytotoxicity assays, fluorescence and confocal microscopy images are available in the supplementary information (SI).

View Article Online
DOI: 10.1039/D6OB00581K

Acknowledgements

The authors thank Dr. Ebert in ETH for his help in ESR and NMR measurements. The authors thank Prof. Leroux in ETH for his help in fluorescence measurements. The authors thank Prof. Bode in ETH for his help in CD and UV-vis measurements. ScopeM of ETH, MoBiAS and the NMR service in the D-CHAB at ETH are acknowledged for their help in the measurements.
This research was supported by SNF Strategic Japanese-Swiss Science and Technology Program (IZLJZ2_183660, Y.Y.), JSPS under the Joint Research Program implemented in association with SNF (20191508, H.M. and N.Y.-S.), SNF Project Funding (205321_173018, Y.Y.), ETH Research Grants (ETH-21_15-2; ETH-36_20-2, Y.Y.), and JSPS KAKENHI (Grant-in-Aid for Scientific Research [A], 6251004, H.M.; Grants-in-Aid for Scientific Research on Innovative Areas, 21H00264, 22H04707, H.M.; Grant-in-Aid for Scientific Research [C], 15K07164, N.Y.-S.).

Notes and references

1. N. V. Anantha, M. Azam and R. D. Sheardy, *Biochemistry*, 1998, **37**, 2709-2714.
2. C. L. Grand, H. Han, R. M. Muñoz, S. Weitman, D. D. Von Hoff, L. H. Hurley and D. J. Bearss, *Mol. Cancer Ther.*, 2002, **1**, 565-573.
3. I. M. Dixon, F. Lopez, A. M. Tejera, J.-P. Estève, M. A. Blasco, G. Pratviel and B. Meunier, *J. Am. Chem. Soc.*, 2007, **129**, 1502-1503.
4. U. Chilakamarthi, D. Koteshwar, S. Jinka, N. Vamsi Krishna, K. Sridharan, N. Nagesh and L. Giribabu, *Biochemistry*, 2018, **57**, 6514-6527.
5. M. Gunaratnam, M. d. l. Fuente, S. M. Hampel, A. K. Todd, A. P. Reszka, A. Schätzlein and S. Neidle, *Bioorg. Med. Chem.*, 2011, **19**, 7151-7157.
6. S. Asamitsu, S. Obata, Z. Yu, T. Bando and H. Sugiyama, *Molecules*, 2019, **24**, 429.
7. T.-M. Ou, Y.-J. Lu, C. Zhang, Z.-S. Huang, X.-D. Wang, J.-H. Tan, Y. Chen, D.-L. Ma, K.-Y. Wong, J. C.-O. Tang, A. S.-C. Chan and L.-Q. Gu, *J. Med. Chem.*, 2007, **50**, 1465-1474.
8. P. Podbevšek and J. Plavec, *Nucleic Acids Res*, 2016, **44**, 917-925.
9. R. Chaudhuri, S. Bhattacharya, J. Dash and S. Bhattacharya, *J. Med. Chem.*, 2021, **64**, 42-70.
10. V. Caprio, B. Guyen, Y. Opoku-Boahen, J. Mann, S. M. Gowan, L. M. Kelland, M. A. Read and S. Neidle, *Bioorg. Med. Chem. Lett.*, 2000, **10**, 2063-2066.
11. I. M. Dixon, F. Lopez, J.-P. Estève, A. M. Tejera, M. A. Blasco, G. Pratviel and B. Meunier, *ChemBioChem*, 2005, **6**, 123-132.
12. L. Finlayson, I. R. M. Barnard, L. McMillan, S. H. Ibbotson, C. T. A. Brown, E. Eadie and K. Wood, *Photochem. Photobiol.*, 2022, **98**, 974-981.
13. P. Agostinis, K. Berg, K. A. Cengel, T. H. Foster, A. W. Girotti, S. O. Gollnick, S. M. Hahn, M. R. Hamblin, A. Juzeniene, D. Kessel, M. Korbelik, J. Moan, P. Mroz, D. Nowis, J. Piette, B. C. Wilson and J. Golab, *CA: A Cancer J. Clinic.*, 2011, **61**, 250-281.
14. H. Abrahamse and Michael R. Hamblin, *Biochem. J.*, 2016, **473**, 347-364.
15. M. Deiana, José M. Andrés Castán, P. Josse, A. Kahsay, Darío P. Sánchez, K. Morice, N. Gillet, R. Ravindranath, Ankit K. Patel, P. Sengupta, I. Obi, E. Rodriguez-Marquez, L. Khrouz, E. Dumont, L. Abad Galán, M. Allain, B. Walker, H. S. Ahn, O. Maury, P. Blanchard, T. Le Bahers, D. Öhlund, J. von Hofsten, C.

View Article Online
DOI: 10.1039/D6OB00581K

Monnereau, C. Cabanetos and N. Sabouri, *Nucleic Acids Res.*, 2023, **51**, 6264-6285.
16. X. Zhang and M.-H. Hu, *Sens. Actu. B: Chem.*, 2025, **425**, 136952.
17. D. Lin, W. Long, B. Zheng, J. Zhu, H. Yang, G. Song, D. Yan, Y. Liu, L. Wang, D. Wang and B. Z. Tang, *Sens. Actu. B: Chem.*, 2026, **448**, 139052.
18. X.-D. Wang, J.-H. Lin and M.-H. Hu, *J. Biol. Chem.*, 2026, **302**, 111181.
19. Q. Wu, W.-W. Hong, J.-H. Shi, R.-S. Deng, W.-Q. Chen, C.-L. Yuan and W.-J. Mei, *Aggregate*, 2026, **7**, e70239.
20. Y. Dong and M. H. Hu, *Eur. J. Med. Chem.*, 2026, **302**.
21. X. D. Wang, Y. S. Liu, Z. L. Liang and M. H. Hu, *Eur. J. Med. Chem.*, 2025, **289**.
22. X. Zhang, J. X. Wang and M. H. Hu, *ACS Pharmacol. Transl.*, 2024, **7**, 2174-2184.
23. G. Biffi, D. Tannahill, J. McCafferty and S. Balasubramanian, *Nat. Chem.*, 2013, **5**, 182-186.
24. R. Hänsel-Hertsch, D. Beraldi, S. V. Lensing, G. Marsico, K. Zyner, A. Parry, M. Di Antonio, J. Pike, H. Kimura, M. Narita, D. Tannahill and S. Balasubramanian, *Nat. Genet.*, 2016, **48**, 1267-1272.
25. R. Hänsel-Hertsch, M. Di Antonio and S. Balasubramanian, *Nat. Rev. Mol. Cell. Biol.*, 2017, **18**, 279-284.
26. J. An, M. Yin, J. Yin, S. Wu, C. P. Selby, Y. Yang, A. Sancar, G.-L. Xu, M. Qian and J. Hu, *Nucleic Acids Res.*, 2021, **49**, 12252-12267.
27. J. Osterloh and M. G. H. Vicente, *J. Porphyrins Phthalocyanines*, 2002, **06**, 305-324.
28. S. Cogoi and L. E. Xodo, *Chem. Commun.*, 2010, **46**, 7364-7366.
29. Ç. Çelik, N. Kakusho, T. Xu, S. Sik Lee, N. Yoshizawa-Sugata, H. Masai and Y. Yamakoshi, *RSC Med. Chem.*, 2026, **17**, 225-235.
30. C. Wei, L. Wang, G. Jia, J. Zhou, G. Han and C. Li, *Biophys. Chem.*, 2009, **143**, 79-84.
31. A. Wolfe, G. H. Shimer and T. Meehan, *Biochemistry*, 1987, **26**, 6392-6396.
32. Y. Kanoh, S. Matsumoto, R. Fukatsu, N. Kakusho, N. Kono, C. Renard-Guillet, K. Masuda, K. Iida, K. Nagasawa, K. Shirahige and H. Masai, *Nat. Struct. Mol. Biol.*, 2015, **22**, 889-897.
33. H. Masai, N. Kakusho, R. Fukatsu, Y. Ma, K. Iida, Y. Kanoh and K. Nagasawa, *J. Biol. Chem.*, 2018, **293**, 17033-17049.
34. A. Ambrus, D. Chen, J. Dai, T. Bialis, R. A. Jones and D. Yang, *Nucleic Acids Res.*, 2006, **34**, 2723-2735.
35. Y. Lion, M. Delmelle and A. Van De Vorst, *Nature*, 1976, **263**, 442-443.
36. O. Kikin, L. D'Antonio and P. S. Bagga, *Nucleic Acids Res.*, 2006, **34**, W676-W682.

View Article Online
DOI: 10.1039/D6OB00581K

Data availability

Supplementary information: experimental data and details regarding the synthesis, ESR, UV-vis, fluorescence and flow cytometry, DNA photocleavage, photocytotoxicity assays, fluorescence and confocal microscopy images are available in the supplementary information (SI).